RSC Advances

PAPER

View Article Online
View Journal | View Issue

Cite this: *RSC Adv.*, 2017, **7**, 24215

Perylene dye-functionalized silver nanoparticles serving as pH-dependent metal sensor systems†

Yan Sun,* Tongfei Zuo, Fang Guo, Jing Sun, Ziwei Liu and Guowang Diao*

Received 20th March 2017
Accepted 19th April 2017

DOI: 10.1039/c7ra03264a

rsc.li/rsc-advances

Lysine-functionalized perylene was used to modify nanoparticles. Due to the benefits from a synergetic effect that originated between the perylene and silver nanoparticles, color-based metal sensor systems were established. At pH = 12.6, Cr^{6+} with a concentration of 100 nM could be detected by a color change from deep yellow to orange; after decreasing the pH to 12.0, the detection limit decreased to 2 μM. Interestingly, after further decreasing the pH to 11.0, another kind of metal ion (Cd^{2+}) could be recognized with a detection concentration of 10 μM. At pH = 10.0, Pb^{2+} with a concentration of 2 μM could be detected.

1. Introduction

Recently, perylene diimide derivatives have received extensive attention due to their various applications in self-assembly,[1] supramolecular polymerization,[2] polymer solar cells,[3] single wall carbon nanotubes,[4] and organic photovoltaics.[5] The properties of these materials are related not only to their own characteristics but also to their interactions with other materials.[6] Therefore, the fabrication of perylene-based composites with tunable functions is of particular importance for making high performance materials.[7] In addition to designing and synthesizing new compounds, improving and optimizing material compositions *via* nanotechnology is an effective and efficient strategy for maximizing material performance using available functional molecules.[8] Nanometer-sized metal materials have attracted a great deal of attention because of their unique chemical and physical properties.[9] Normally, the size, shape and surface modification of metal nanoparticles comprise some of the most important factors that can dramatically affect their properties.[10] To improve their properties, many kinds of molecules have been used for the modification of nanoparticles, including surfactants,[11] amino acids,[12] and macromolecules.[13–15] By virtue of these modification, nanoparticles possess various functions, including heavy metal ion detection.[16] As we know, heavy metal ions pose a serious threat to human health and need to be detected.[17,18] Among them, Cr^{6+} is considered as a severe environmental pollutant due to its carcinogenic nature.[19] The major toxic effects of Cr^{6+} include chronic ulcers, dermatitis, and local effects in lungs.[20] As another kind of toxic heavy metal ion, Cd^{2+} is extremely toxic even in low concentrations.[21,22] Similarly, Pb^{2+} is a toxic substance in the environment due to its wide distribution and use in batteries, gasoline and pigments.[23,24] Even a low level exposure to Pb^{2+} can cause memory loss, muscle paralysis and brain development inhibition, particularly in children, causing various neurotoxic effects.[25] Currently, silver nanoparticles (AgNPs) provide a simple and low-cost solution for the rapid detection of heavy ions.[26–30] However, in most cases, only one kind of heavy metal ion is detected using the above strategy. Moreover, a series of other reagents is also necessary for the selective detection of heavy metal ions.[31–35] To the best of our knowledge, the use of perylene for modifying nanoparticles is still in its initial stages.[36–41] Considering that the optical properties of perylenes depends on their state of aggregation, we envisage that the synergy between perylene and AgNPs will amplify the detection of AgNP-mediated color sensors. Here, the introduction of perylene results in pH-dependent metal sensor selectivity. It is found that the use of other reagents is not required. By simply adjusting the pH of the perylene solution, the as-prepared AgNPs can be used to detect toxic heavy metal ions. Cr^{6+} with a concentration of 100 nM can be detected by the naked eye at a pH = 12.6. Furthermore, Cd^{2+} (pH = 11.0, 10 μM) and Pb^{2+} (pH = 11.0, 2 μM) can be detected selectively by adjusting the pH.

2. Experiments

2.1 Chemicals and characterization

All the glassware used was thoroughly washed with fresh water and then rewashed with Milli-Q water and air dried. 1,6,7,12-Tetrachloroperylene 3,4,9,10-tetracarboxylic acid dianhydride was purchased from commercial sources and was of analytical or reagent grade. Lysine was purchased from Macklin. Other reagents were purchased from Sinopharm Chemical Reagent Co, Ltd (Shanghai) and used without further purification unless otherwise specified. Deionized water was used throughout the

College of Chemistry and Chemical Engineering, Yangzhou University, 225002, China. E-mail: sunyan@yzu.edu.cn; gwdiao@yzu.edu.cn

† Electronic supplementary information (ESI) available. See DOI: 10.1039/c7ra03264a

experiments. All the heavy metal salts were used to prepare stock solutions and were serially diluted to obtain lower concentrations. UV-vis absorption spectra were recorded using a UV-2501 spectrophotometer. The TEM images were obtained using a Philips TECNAI-12 instrument with an accelerating voltage of 120 kV. HRTEM and elemental mapping images were obtained using a Tecnai G2 F30 S-TWIN instrument. Light scattering measurements were conducted on a Malvern Nanosizer S instrument at room temperature.

2.2 Synthesis of silver nanoparticles at different pH values

The synthesis and structure characterization of the (lysine-perylene-lysine) **LPL** was reported elsewhere.[42] **LPL** was initially dissolved in a NaOH solution to form a 200 μM stock solution at pH = 11. Subsequently, 0.15 mL of **LPL** (200 μM) dissolved in 3.85 mL of aqueous solution with pH values of 12.6, 12.0, 11.0, and 10.0. **LPL**-AgNPs were synthesized by the reduction of $AgNO_3$ in the presence of **LPL**. In a typical experiment, $AgNO_3$ (0.5 mL, 10 mM) was added into the solution of **LPL** (20.0 mL, 7.5 μM) at given pH. Subsequently, a fresh $NaBH_4$ solution (0.5 mL, 0.1 M) was added into the solution with rapid stirring.

2.3 Colorimetric detection of various heavy metal ions

A variety of aqueous solutions of ions were added into the as-prepared **LPL**-AgNP solutions. At pH = 12.6, the final concentration of the individual metal ion solutions was 100 nM. At pH = 12.0, the final concentration of the individual metal ion solutions was 2 μM. At pH = 11.0, the final concentration of the individual metal ion solutions was 10 μM. At pH = 10.0, the final concentration of the individual metal ion concentrations was 2 μM.

3. Results and discussion

3.1 Fabrication of perylene capped silver nanoparticles

Scheme 1 shows the chemical structure of the lysine-functionalized perylene (**LPL**). **LPL** possess a bolaamphiphile structure with a hydrophobic rigid perylene backbone as the skeleton and pH-responsive lysine residue as the hydrophilic head. **LPL**-capped AgNPs (**LPL**-AgNPs) were prepared by $NaBH_4$ reduction, using **LPL** as the protective ligand. After the synthesis of the **LPL**-AgNPs, one lysine residue end of the **LPL** was linked to the AgNPs through $-COO^-$ and $-NH_2$ groups, and another lysine residue from the **LPL** protected them from aggregation due to the negatively charged $-COO^-$ electrostatic repulsions under alkaline conditions.

Fig. 1 presents TEM images and histograms of the size distribution of the **LPL**-AgNPs at different pH levels, revealing that the obtained AgNPs were formed and well dispersed at pH 12.6, 12.0, 11.0, and 10.0 (Fig. 1d). The average diameters and standard deviations determined from their histograms were 7.5 ± 2.4 nm, 6.3 ± 2.3 nm, 3.2 ± 1.7 nm, and 7.0 ± 2.2 nm, respectively (Fig. 1 inset). The UV-vis spectra show the absorption band was centered at *ca.* 390 nm, confirming the formation of **LPL**-modified AgNPs, which are consistent with TEM results. The **LPL**-AgNPs were not obtained at pH > 12.6. Thus, pH = 12.6 was the highest value in our study (Fig. S1†).

3.2 LPL-AgNPs as metal ion sensors at different pH values

When metal ions were added to the **LPL**-AgNPs, metal ions could bind to lysine residue easily and act as a crosslinking agent for the **LPL**-AgNPs, thereby inducing aggregation of the AgNPs. Subsequently, the metal ion detection ability of the as-prepared **LPL**-AgNPs at different pH values was studied. At pH = 12.6, the **LPL**-AgNPs were studied separately for each of the metal ions, including monovalent ions (Na^+ and K^+), divalent ions (Mn^{2+}, Cd^{2+}, Pb^{2+}, Ba^{2+}, Zn^{2+} and Ca^{2+}), trivalent ions (Al^{3+}) and hexavalent ions (Cr^{6+}) at a fixed concentration (100 nM). As shown in Fig. 2a, the **LPL**-AgNPs turned from orange brown to orange after the addition of Cr^{6+}, whereas the **LPL**-AgNPs remained orange brown upon interacting with interfering ions.

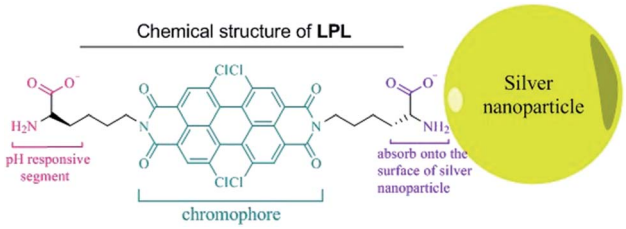

Scheme 1 Chemical structure of the **LPL** at pH > 10.

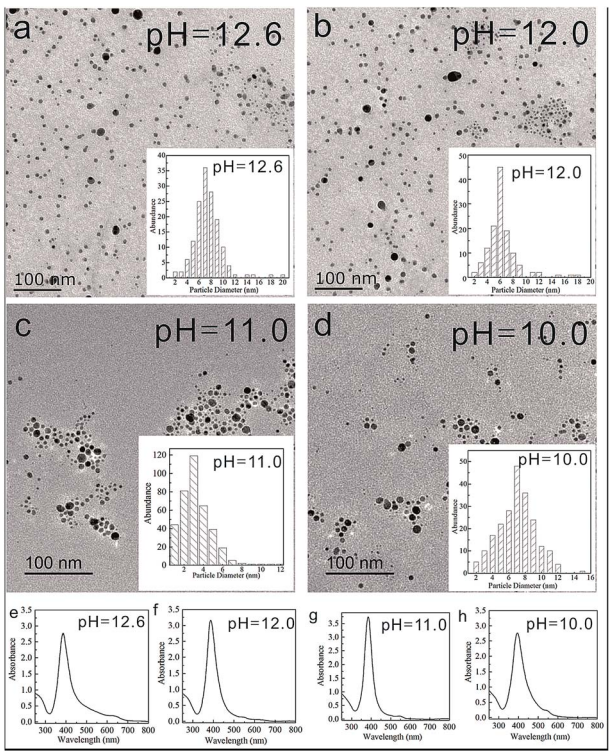

Fig. 1 TEM images of the **LPL**-AgNPs at pH (a) 12.6, (b) 12.0, (c) 11.0, and (d) 10.0. (Inset) Corresponding histograms of the size distribution and (e)–(h) corresponding UV-vis spectra.

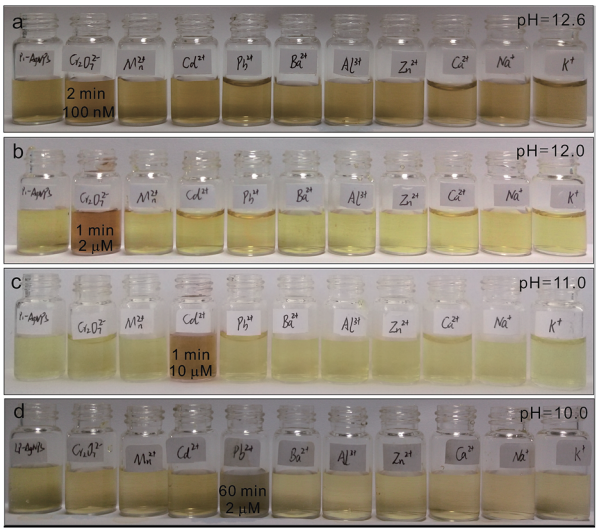

Fig. 2 (a) Digital images of the **LPL**-AgNPs after the addition of different metal ions (100 nM) at pH = 12.6. (b) Digital images of the **LPL**-AgNPs after the addition of different metal ions (2 μM) at pH = 12.0. (c) Digital images of the **LPL**-AgNPs after the addition of different metal ions (10 μM) at pH = 11.0. (d) Digital images of **LPL**-AgNPs after the addition of different metal ions (2 μM).

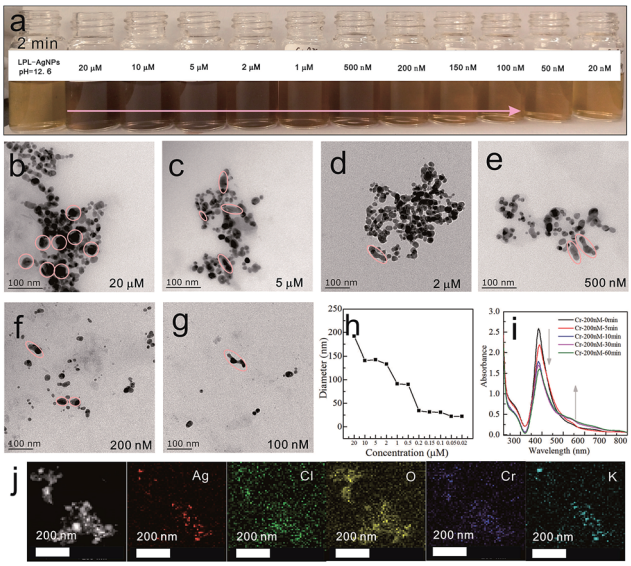

Fig. 3 (a) Digital image of **LPL**-AgNPs interacting with different concentrations of Cr^{6+}. (b)–(g) TEM images of the **LPL**-AgNPs after interacting with Cr^{6+} at concentrations of 10 μM, 2 μM, 200 nM, and 100 nM. (h) Evolution of the diameter of the **LPL**-AgNPs. (i) UV-vis spectra of the **LPL**-AgNPs with time. (j) Left: STEM image of the **LPL**-AgNPs-Cr^{6+}. Right: the corresponding mapping images.

Compared to the other ions, which had no obvious effect on the absorbance of the **LPL**-AgNPs, the absorbance after the addition of Cr^{6+} was dramatic decreased (Fig. S2a,† red line). The only difference is that the ratio of $A_{545/384}$ for the Cr^{6+} was close to 0.30, which was higher than that of other metal ions (Fig. S2e†). After decreasing the pH to 12.0, a similar selectivity for Cr^{6+} was observed but the detection limit decreased to 2 μM (Fig. 2b).

The peak at approximately 390 nm decreased obviously, and a new peak at approximately 500 nm appeared (Fig. S2b,† red line). The ratio of $A_{503/390}$ for Cr^{6+} (*ca.* 0.60) was much higher than others (Fig. S2f†), demonstrating that the **LPL**-AgNPs had a very high specificity toward Cr^{6+} in strong basic conditions. Further decreasing the pH to 11.0, the **LPL**-AgNPs showed a selective color change from yellow to dark orange after the addition of Cd^{2+} (Fig. 2c, detection limit: 10 μM), and the peak at approximately 388 nm decreased slightly (Fig. S2c,† pink line). It was found that while the ratio change existed for the other metal ions (Fig. S2g†), the ratio of $A_{551/388}$ for Cd^{2+} was approximately 0.16, which was much higher than that of other metal ions (below 0.07). For the **LPL**-AgNPs at pH = 10.0, the color changed to dark after the addition of Pb^{2+} (Fig. 2d, detection limit: 2 μM), and the peak at approximately 390 nm decreased obviously (Fig. S2d,† green line). The ratio of $A_{548/388}$ for Pb^{2+} was approximately 0.15 (higher than that of the other metal ions), revealing that the **LPL**-AgNPs had a very high specificity toward Pb^{2+} (Fig. S2h†). It should be noted that, as long as the action time is long enough, the addition of most ions can cause discoloration.

To obtain further insight into the color change at a given pH, Cr^{6+} solutions with different concentrations were added into the **LPL**-AgNP solutions (pH = 12.6). As shown in Fig. 3a, a fine gradation in the color development from brown to dark orange was recorded. TEM images of the **LPL**-AgNPs after the addition of Cr^{6+} with concentrations of 20 μM, 5 μM, 2 μM, 500 nM, 200 nM, and 100 nM, as shown in Fig. 3b–g, further confirm that the observed color changes were the result of **LPL**-AgNP aggregation induced by Cr^{6+} (pink circles). The DLS data clearly indicate that the hydrodynamic diameter increased as a function of the Cr^{6+} concentration (Fig. 3h), which was consistent with color changes. The UV-vis spectra were examined at 0, 5, 10, 30, and 60 min, as shown in Fig. 3i. As the incubation time increased, the absorption at 384 nm continuously decreased and a new absorption band appeared at approximately 545 nm, which was caused by the coordination between Cr^{6+} and the **LPL**-AgNPs.

It should be mentioned that excess reducing borohydride in the **LPL**-AgNPs solution was responsible for reducing Cr^{6+} to Cr^{3+}, which in turn interacted with the **LPL**-AgNPs. Thus, it was deduced that Cr^{3+} instead of Cr^{6+} was participating in the coordination.[43] The elemental mapping analysis indicated a homogeneous distribution of Cl and O, which are characteristic elements of the **LPL** (Fig. 3j), providing further evidence of the **LPL**-capped AgNP formation. Importantly, Cr^{6+}-induced aggregations were evidenced by the homogeneous distribution of Cr and K (from $K_2Cr_2O_7$) across the aggregates (Fig. S3†).

After, different concentrations of Cd^{2+} solutions ranging from 20 μM to 20 nM were added into the **LPL**-AgNP solutions (pH = 11.0). Fig. 4a shows that the color changed from yellow to brown after the addition of Cd^{2+}, and aggregates were formed after interacting with Cd^{2+} (Fig. 4b and c). The DLS data indicate that the hydrodynamic diameter increased as a function of the Cd^{2+} concentration (Fig. 4d); the UV-vis spectra demonstrate that the aggregation behavior of the **LPL**-AgNPs was highly

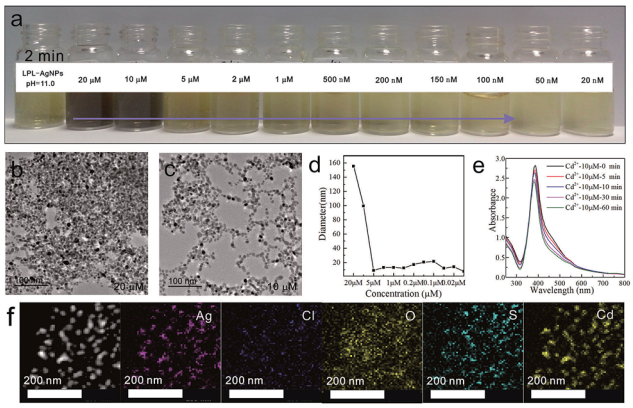

Fig. 4 (a) Digital image of **LPL**-AgNPs interacting with Cd^{2+}. (b and c) TEM images of the **LPL**-AgNPs after interacting with Cd^{2+} at concentrations of 20 μM and 10 μM. (d) Evolution of the diameter of the **LPL**-AgNPs. (e) UV-vis spectra of the **LPL**-AgNPs with time. (f) Left: STEM image of the **LPL**-AgNPs-Cd^{2+}. Right: the corresponding mapping images.

dependent on the incubation time (Fig. 4e). The elemental mapping analysis indicated a homogeneous distribution of Cl and O, which are characteristic elements of the **LPL** (Fig. 4f and S4†).

More importantly, Cd^{2+}-induced aggregations were indicated by the homogeneous distribution of Cd and S (from $CdSO_4$) across the aggregates. Interestingly, after decreasing the pH to 10.0, the **LPL**-AgNPs shifted their selective detection ability to Pb^{2+}. As shown in Fig. 5a, a fine gradation in the color development was recorded from yellow to slight brown after the addition of Pb^{2+}. It was observed that after interacting with the Pb^{2+} solution (20 μM), large aggregates in size range from 90 nm to 100 nm were formed (Fig. 5b and c). The above changes were attributed to the Pb^{2+} induced aggregation (green circles), which revealed fused particles with sizes that depended on the

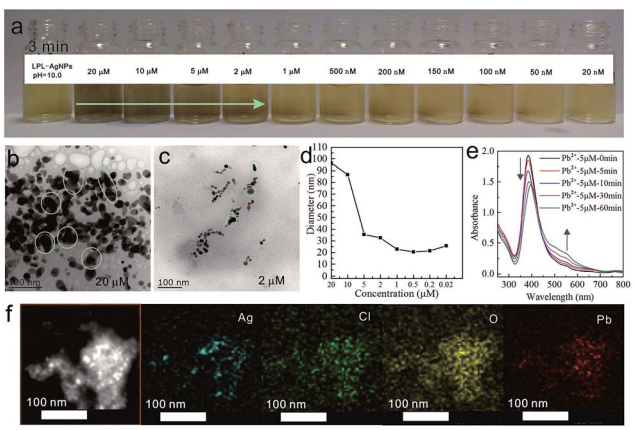

Fig. 5 (a) Digital image of **LPL**-AgNPs interacting with different concentrations of Pb^{2+}. (b and c) TEM images of **LPL**-AgNPs after interacting with Pb^{2+} at the concentrations of 20 μM and 2 μM. (d) Evolution of the diameter of the **LPL**-AgNPs with the concentration. (e) UV-vis spectra of **LPL**-AgNPs with time. (f) Left: STEM image of the **LPL**-AgNPs-Pb^{2+}. Right: the corresponding mapping images.

concentration of Pb^{2+}. The DLS data clearly show aggregation of the **LPL**-Ag NPs as a function of the Pb^{2+} concentration (Fig. 5d), which was responsible for the gradation of the color development. The change in the intensity of the absorbance was monitored and captured by the UV–vis spectra, as shown in Fig. 5e. The absorbance centered at 390 nm shifted to the right, forming a distinct second peak at approximately 550 nm. This second peak could be ascribed to the complex formed due to the aggregation of the particles. The elemental mapping analysis demonstrated a homogeneous distribution of Cl and O (Fig. 5f). Furthermore, Pb^{2+}-induced aggregations were evidenced by the homogeneous distribution of Pb^{2+} across the aggregates (Fig. S5†).

3.3 Mechanism

The driving force for the metal ion-probe affinity might be coordination interaction. Take the interaction between Cd^{2+} and LPL for example. For the powder sample (have no interaction with heavy metal ions), the peak of C=O and C–N bond was observed at 1660 cm^{-1} and 1176 cm^{-1}. After the interaction with heavy metal ions, the C=O and C–N bond was decreased to 1626 cm^{-1} and 1095 cm^{-1}, respectively (Fig. S6†). The decrease of wave numbers demonstrated the interaction of amino and carboxyl with Cd^{2+}.[44] More importantly, the selective color changes could be explained well by the metal ion mediated aggregation at a given pH. To determine the essential factor of the as-prepared sensor system, a series of control experiments was conducted, which demonstrated that efficient detection could not be realized by lysine, **LPL**, or lysine-modified AgNPs alone. As shown in Fig. S7b,† the lysine solution did not show any response before and after the addition of Cr^{6+} at pH = 12.6 (Fig. S7a†). Similarly, the lysine-functionalized perylene solution exhibited a colorless appearance before and after the addition of Cr^{6+} at pH = 12.6. Furthermore, the **LPL** exhibited no selective colorimetric sensing in response to all the ions in an aqueous solution at pH = 12.0. The interactions between Cr^{6+} with lysine and Cr^{6+} with **LPL** at other pH values (12.0, 11.0, and 10.0) was similar to the interactions at pH = 12.6 (Fig. S8–S10†). Furthermore, the lysine-modified AgNPs exhibited no selective colorimetric sensing in response to all the ions in aqueous solutions at pH > 12.0, pH = 11.0, and pH = 10.0. It is should be mentioned that the lysine-AgNPs could not be obtained at pH > 12.0. Thus, the detection ability of the lysine-AgNPs at only pH = 11.0 and pH = 10.0 was investigated. At pH = 11.0, after the addition of metal ions into the lysine-AgNP solution, no selective colorimetric sensing occurred. For a continuous decrease in the concentration of metal ions to 100 nM, no color change was observed among all the different ions (Fig. S11–S12†).

As shown in Fig. 6a, at pH = 12.6, no obvious absorbance decrease was observed, except for Cr^{6+} and Cr^{3+}, resulting in the selective detection ability for Cr^{6+} at short time scales. At pH = 12.0, a dramatic decrease was only observed for Cr^{6+} and Cr^{3+} (Fig. 6b), demonstrating that the detection arises from the fast kinetic rate. Similarly, at pH = 11.0 and 10.0, when compared with the other metal ions, the **LPL**-AgNPs-M (M = Cd^{2+}, at pH =

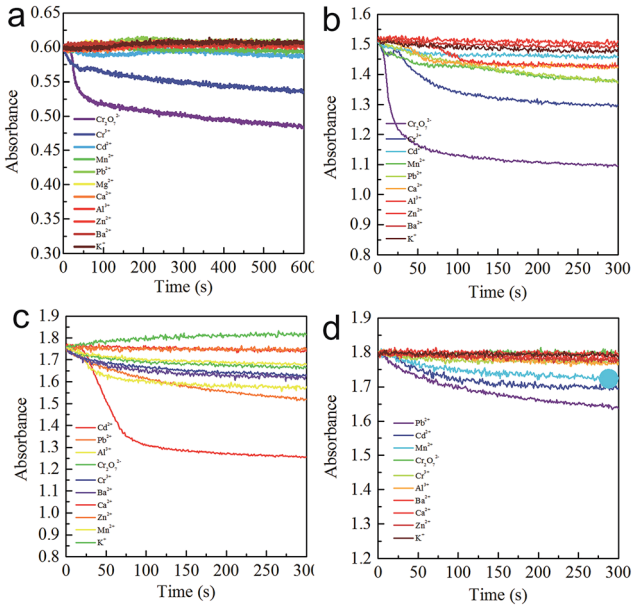

Fig. 6 Aggregation kinetics of the various metal ions at pH (a) 12.6, (b) 12.0, (c) 11.0, and (d) 10.0.

11.0; M = Pb^{2+}, at pH = 10.0) showed a consistent absorbance decrease (Fig. 6c and d), which resulted from the different kinetic rates. The different coordination rates might have resulted from the different states at each given pH. It is well known that the dissociation constant of $-COO^-$ is influenced by different pH values. As we know, $pK_{a1} = 2.18$, $pK_{a2} = 8.95$, and $pK_{a3} = 10.53$. Furthermore, it is reported that all carboxyl groups are ionized to $-COO^-$ at pH > 10, the difference is that the ionization state of the amine at different pH.[45] Based on the literature and calculation, at pH = 10, $-NH_3^+$ (40%) and $-NH_2$ (60%) coexisted, increase the pH to 11, it is deduced that $-NH_3^+$ (<40%) and $-NH_2$ (>60%) coexisted, at pH > 12, all the existed as $-NH_2$. The fluorescence spectra of the **LPL**, **LPL**-AgNPs, and **LPL**-AgNPs-M (Cr^{6+}, Cd^{2+}, and Pb^{2+}) were recorded to determine the **LPL** state.

As shown in Fig. S13a and b,† the **LPL** exhibited only one peak at pH = 12.6 and 12.0, which indicated that the complete dissociation of the carboxyl groups occurred and the **LPL** existed as a free molecule, in turn, facilitating the interaction between metal ions and AgNPs. However, the **LPL** exhibited two peaks at pH = 11.0 and 10.0, indicating that the **LPL** existed as a slightly aggregated state[42] at this condition, which might have decreased the detection limit of the AgNPs. Based on above results, we deduced the selective color sensor mechanism. As shown in Scheme 2 (Fig. S14†), at strong basic conditions, Cr^{6+} was reduced to Cr^{3+}, which can act as a crosslinking agent for the **LPL**-AgNPs. Negative carboxylate anions of the **LPL** on the AgNP surface can be attracted together by a carboxylate-Cr^3-carboxylate linker. One Cr^{3+} could be chelated with three **LPL** molecules by one $-NH_2$ and one $-COO^-$ group from each **LPL** molecule at pH 12.6 and 12.0.[46] At pH = 10.0, $-NH_3^+$ (40%) and $-NH_2$ (60%) coexisted,[45] it is deduced that **LPL** could easily coordinate with Pb^2 at this condition. At pH = 11.0, $-NH_3^+$

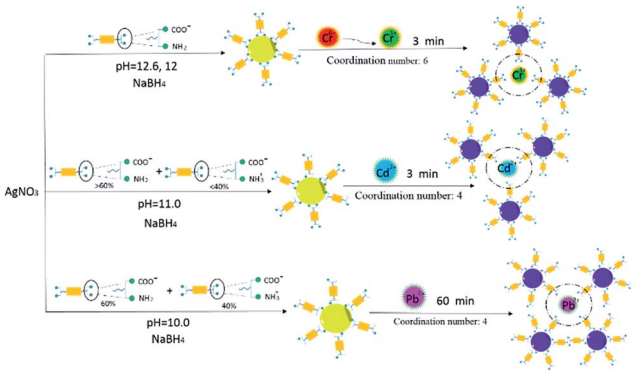

Scheme 2 Possible mechanisms of the interactions between the metal ions and **LPL**-AgNPs. The ratio (>60%, and <40% at pH = 11.0) was calculated based on the literature.[44]

(<40%) and $-NH_2$ (>60%) coexisted (the ratio was calculated based on the literature[45]), it is supposed that this difference might result in different kinetic when reacting with Cd^{2+}. As mentioned above, the detection limit for Cr^{6+} is 100 nM at pH = 12.6 and 2 μM at pH = 12.0. Furthermore, the detection limit for Cd^{2+} is 10 μM at pH = 11.0 and detection limit for Pb^{2+} is 10 μM at pH = 11.0. Compared with the literature,[26,35] different ions could be detected by changing the pH of LPL, but the detection sensitivity is not as good as reported in the literature. Considering various reagents were used in the reported system, complicated adjustment could be conducted for improving the detection limit is different from our system.

4. Conclusions

Herein, we synthesized **LPL**-AgNPs as probes for toxic metal ions with high sensitivity and selectivity. **LPL** endowed as-prepared silver nanoparticles with pH-dependent properties, exhibiting selective colorimetric sensing of toxic Cr^{6+}, Cd^{2+}, and Pb^{2+} metal ions in aqueous solutions at different pH values. More importantly, the synergetic effect between the lysine-functionalized perylene and AgNPs amplified the color change and then improved the pH-dependent selectivity. In view of the simple modification, low cost, user-friendliness and bare-eye visual readout, these perylene modified AgNPs have the potential to be used for the detection of Cr^{6+}, Cd^{2+}, and Pb^{2+}.

Acknowledgements

This work was supported by the National Natural Science Foundation of China (21503185 and 21273195), China Postdoctoral Science Foundation (137070124). Electronic Supplementary Information (ESI) is available: characterizations of nanoparticles detection.

References

1 M. Frank, J. Ahrens, I. Bejenke, M. Krick, D. Schwarzer and G. H. Clever, *J. Am. Chem. Soc.*, 2016, **138**, 8279–8287.

2 S. Ogi, V. Stepanenko, J. Thein and F. Würthner, *J. Am. Chem. Soc.*, 2016, **138**, 670–678.
3 L. Nian, W. Zhang, N. Zhu, L. Liu, Z. Xie, H. Wu, F. Würthner and Y. Ma, *J. Am. Chem. Soc.*, 2015, **137**, 6995–6998.
4 Y. Tsarfati, V. Strauss, S. Kuhri, E. Krieg, H. Weissman, E. Shimoni, J. Baram and D. Guldi, *J. Am. Chem. Soc.*, 2015, **137**, 7429–7440.
5 S. Holliday, R. S. Ashraf, C. B. Nielsen, M. Kirkus, J. A. Röhr and C. H. Tan, *J. Am. Chem. Soc.*, 2015, **137**, 898–904.
6 Y. Sun, C. G. Yan, Y. Yao, Y. Han and M. Shen, *Adv. Funct. Mater.*, 2008, **18**, 3981–3990.
7 Y. Sun, W. Fu, Z. Li and Z. Wang, *Langmuir*, 2014, **30**, 8615–8620.
8 Y. Sun, F. Guo, T. Zuo, J. Hua and G. Diao, *Nat. Commun.*, 2016, **7**, 12042.
9 A. Henglein, *Chem. Rev.*, 1989, **89**, 1861–1873.
10 Z. Niu and Y. Li, *Chem. Mater.*, 2014, **26**, 72–83.
11 M. Shen, Y. Sun, Y. Han, R. Yao and C. G. Yan, *Langmuir*, 2008, **24**, 13161–13167.
12 D. Li, Y. Dong, B. Y. Li, Y. Wu, K. Wang and S. C. Zhang, *Analyst*, 2015, **140**, 7672–7677.
13 Y. Sun, Y. Yao, C. G. Yan, Y. Han and M. Shen, *ACS Nano*, 2010, **4**, 2129–2141.
14 Y. Yao, M. Xue, M. Z. Zhang, Y. Wang and F. Huang, *Chem. Sci.*, 2013, **4**, 3667.
15 Y. Yao, Y. Wang and F. Huang, *Chem. Sci.*, 2014, **5**, 4312.
16 Y. Gao, J. Xin, Z. Shen, W. Pan, X. Li and A. Wu, *Sens. Actuators, B*, 2013, **181**, 288–293.
17 L. Zhang, C. Xu and B. Li, *Microchim. Acta*, 2009, **166**, 61–68.
18 B. Valeura and L. Leray, *Coord. Chem. Rev.*, 2000, **205**, 3–40.
19 H. G. Preuss, B. Echard, N. V. Perricone, D. Bagchi, T. Yasmin and S. J. Stohs, *J. Inorg. Biochem.*, 2008, **102**, 1986–1990.
20 R. F. M. Herber and M. Stoeppler, *Trace Element Analysis in Biological Specimens, Vol. 15,(Techniques and Instrumentation in Analytical Chemistry)*, Elsevier Science, 1st edn, 1994.
21 S. Haouema, N. Hmada, F. M. Najjarb, E. A. Hania and R. Saklyc, *Exp. Toxicol. Pathol.*, 2007, **59**, 77–80.
22 C. D. Klaassen, J. Liu and S. Choudhuri, *Annu. Rev. Pharmacol.*, 1999, **39**, 267.
23 W. Jedrychowski, F. Perera, J. Jankowski, V. Rauh, E. Flaka, K. L. Caldwelld, R. L. Jonesd, A. Paca and I. Lisowska-Miszczyk, *Int. J. Hyg. Environ. Health*, 2008, **211**, 345–351.
24 B. Valeura and L. Leray, *Coord. Chem. Rev.*, 2000, **205**, 3–40.
25 H. Needleman, *Annu. Rev. Med.*, 2004, **55**, 209–222.
26 Y. Zhou, H. Zhao, C. Li, P. He, W. B. Peng, L. F. Yuan, L. X. Zeng and Y. J. He, *Talanta*, 2012, **97**, 331–335.
27 N. Singh, N. Kaur, C. N. Choitir and J. F. Callan, *Tetrahedron Lett.*, 2006, **50**, 4201–4204.
28 R. Hu, L. Zhang and H. B. Li, *New J. Chem.*, 2014, **38**, 2237–2240.
29 Y. Gao, J. Xin, Z. Shen, W. Pan, X. Li and A. Wu, *Sens. Actuators, B*, 2013, **181**, 288–293.
30 F. Kim, J. H. Song and P. Yang, Photochemical, *J. Am. Chem. Soc.*, 2002, **124**, 14316.
31 M. Zhang, Y. Q. Liu and B. C. Ye, *Analyst*, 2012, **137**, 601–607.
32 Z. Chen, L. Chu, C. Liu and S. Luo, *J. Nanosci. Nanotechnol.*, 2015, **15**, 1480–1485.
33 J. Xin, F. Zhang, Y. Gao, Y. Feng, S. Chen and A. Wu, *Talanta*, 2012, **101**, 122–127.
34 T. Wu, C. Liu, K. J. Tan, P. P. Hu and C. Z. Huang, *Anal. Bioanal. Chem.*, 2010, **397**, 1273–1279.
35 W. Jin, P. Huang, F. Wu and L. H. Ma, *Analyst*, 2015, **140**, 3507–3513.
36 D. L. Liao, J. Chen, H. P. Zhou, Y. Wang, Y. X. Li and C. Yu, *Anal. Chem.*, 2013, **85**, 2667–2672.
37 Y. Wang, J. Chen, Y. Chen, W. Y. Li and C. Yu, *Anal. Chem.*, 2014, **86**, 4371–4378.
38 H. P. Jiao, J. Chen, W. Y. Li, F. Y. Wang, H. P. Zhou, Y. X. Li and C. Yu, *ACS Appl. Mater. Interfaces*, 2014, **6**, 1979–1985.
39 R. Hu, T. Liu, X. B. Zhang, S. Y. Huan, C. Wu, T. Fu and W. H. Tan, *Anal. Chem.*, 2014, **86**, 5009–5016.
40 A. K. Dwivedi, M. Pandeeswar and T. Govindaraju, *ACS Appl. Mater. Interfaces*, 2014, **6**, 21369–21379.
41 Y. Y. Lin, R. Chapman and M. M. Stevens, *Anal. Chem.*, 2014, **86**, 6410–6417.
42 Y. Sun, Z. Li and Z. Wang, *J. Mater. Chem.*, 2012, **22**, 4312–4318.
43 A. Ravindrana, M. Elavarasia, T. C. Prathna, A. M. Raichur, N. Chandrasekarana and A. Mukherjee, *Sens. Actuators, B*, 2012, 365–371.
44 K. Fujiwara, A. Ramesh, T. Maki, H. Hasegawa and K. Ueda, *J. Hazard. Mater.*, 2007, **146**, 39–50.
45 N. Kitadai, T. Yokoyama and S. Nakashima, *J. Colloid Interface Sci.*, 2009, **329**, 31–37.
46 C. A. McAuliffe, J. V. Quagliano and L. M. Vallarino, *Inorg. Chem.*, 1966, **5**, 1997–2003.

